Stokes-parameter representation for Compton scattering of entangled and classically correlated two-photon systems

P. Caradonna [*], I. D'Amico, D. G. Jenkins, and D. P. Watts

School of Physics, Engineering and Technology, The University of York, YO10 5DD, York, United Kingdom

A Stokes parameter representation for two-photon systems is developed to calculate cross sections for both entangled and classically correlated mixed states scattering off unpolarized and polarized Compton electrons. The cross section of Compton scattering for pairs of maximally entangled annihilation photons, generated by the disintegration of para-positronium, is compared with classical analogs. An analysis of the symmetrical properties and basis independence of these systems is conducted to elucidate the observed differences. We propose a method to establish an upper bound for identifying correlations influenced by entanglement. Furthermore, we calculate the cross section for Compton scattering of annihilation photons from spin-polarized electrons. A qualitative analysis reveals a contradiction to the contemporary assumption that Compton scattering acts as an entanglement kill switch. These findings contribute to a broader understanding of photon systems and their behavior in various scattering scenarios. Although the primary focus of this article is on Compton scattering, the formalism can be adapted to other interactions, provided that the Mueller matrix representation of the interaction is available.

I. INTRODUCTION

In the past decade, there has been a renewed focus on 0.511-MeV polarization entangled annihilation photons, both at a foundational level [1] and in the understanding of the information content arising from the polarization entanglement of these photons and its potential practical uses. The latter is motivated in large part by the potential application to the development of quantum-entangled positron emission tomography (QE-PET) [2,3].

In practical applications, widely employed materials used for polarization filters face limitations in their efficacy at extremely short wavelengths found in the x-ray or gamma-ray range. Notably, gamma rays at MeV energies have wavelengths on the order of the Compton wavelength of the electron. The exceptionally short wavelengths introduce physical barriers that impede the development of polarization filters for sampling the state of polarization of both nonentangled and entangled gamma rays.

As a result, polarization filters capable of sampling the state of polarization at these wavelengths currently do not exist. In the absence of such filters, Compton scattering offers an alternative statistical method for detecting polarization. This approach indirectly analyzes the polarization state of incident photons by studying the distribution of scattered photons, providing valuable insights into the polarization properties at MeV energies [4–6].

For these reasons, QE-PET uses Compton polarimeters to analyze the information content of entangled annihilation photons. These devices fall into the category of position-sensitive devices capable of determining the trajectory of a scattering photon [7–9]. They achieved this by pinpointing the locations within the device where an incoming photon undergoes Compton scattering and photoelectric absorption. The scattered trajectory is represented by the vector that passes through these two interaction points. With the incident trajectory of a photon known, the incident and scattered photon trajectories enable the determination of the orientation of the scattering plane. In coincidence mode, two Compton polarimeters can be employed to indirectly measure the impact of polarization entanglement on the scattering distributions of two-photon systems. This is achieved by measuring the coincident count rates as a function of the relative azimuthal angle between the scattering planes [10,11].

However, because of the absence of a detailed theory, the impact of Compton scattering on the entanglement between annihilation photons remains inadequately understood. Prevailing assumptions take the conservative position that a single Compton scattering event of an annihilation photon results in the total loss of entanglement [2,12]. The heightened interest in the dynamic role that Compton scattering plays in the entanglement of annihilation photons underscores the need for a comprehensive theory to address this fundamental question.

In both classical and quantum optics, Stokes parameters have proven valuable in characterizing quantum entanglement [13–18]. Expanding on their versatile applications and building on the work of Wightman [19], Fano [20], and McMaster

---

[21], this article utilizes Stokes parameters to establish a theoretical framework for the initial stage of modeling Compton scattering involving a two-photon system in an entangled or classically correlated state to bridge the gap between theory and experiment.

II. PRELIMINARIES

We use the particle physics representation employed by Schmidt and Simons [22] to derive various cross sections for Compton scattering. This representation adopts the right circularly polarized state $|R\rangle$ and the left circularly polarized state $|L\rangle$ as the operational basis. These bases are associated with the σ_3 Pauli matrix, which gives the spin projection of a photon along its trajectory, taking values of ± 1 units of spin angular momentum. The definitions of the circular polarization states $|R\rangle$ and $|L\rangle$, along with the σ_3 matrix, are as follows:

$$|R\rangle = \begin{bmatrix} 1 \\ 0 \end{bmatrix}, \quad |L\rangle = \begin{bmatrix} 0 \\ 1 \end{bmatrix}, \quad \text{and,} \quad \sigma_3 = \begin{bmatrix} 1 & 0 \\ 0 & -1 \end{bmatrix}. \quad (1a)$$

By combining $|R\rangle$ and $|L\rangle$ states in different amounts and phases we obtain other polarization basis sets such as the vertical $|V\rangle$ and horizontal $|H\rangle$ set, and the diagonal $|+45\rangle$ and antidiagonal $|-45\rangle$ basis set, where

$$|V\rangle = \frac{1}{\sqrt{2}} \begin{bmatrix} 1 \\ 1 \end{bmatrix}, \quad |H\rangle = \frac{1}{\sqrt{2}} \begin{bmatrix} 1 \\ -1 \end{bmatrix} \quad (1b)$$

and

$$|\pm 45\rangle = \frac{1}{\sqrt{2}} \begin{bmatrix} 1 \\ \pm i \end{bmatrix}. \quad (1c)$$

The kets $|V\rangle$, $|H\rangle$, and $|\pm 45\rangle$ are in states of indefinite spin angular momentum since they are in a superposition of $|R\rangle$ and $|L\rangle$ states with equal probability of one of these operational bases being observed.

We adopt the McMaster coordinate system convention [21] to define the kinematics of Compton scattering; see Fig. 1. The state of polarization of an incident photon γ_i is defined in the x-y plane of a coordinate system in which the direction of travel of an incident photon is along the z axis, having the unit vector $\hat{z}$. The Compton scatter angle θ is the angle between the trajectory with unit vector $\hat{n}$ of the scattered photon γ_f and the $\hat{z}$ such that $\hat{z} \cdot \hat{n} = \cos\theta$. The kinetic energies of the photons are expressed in units of $mc^2 = 511$ keV where $\hbar, c = 1$. This means, for example, $E_0 = 1$ for photons with an incident energy of 511 keV. The energy of the Compton scattering photon $E(\theta)$ is given by the Compton relation formula

$$E(\theta) = \frac{E_0}{1 + E_0(1 - \hat{z} \cdot \hat{n})} = \frac{E_0}{1 + E_0(1 - \cos\theta)}. \quad (2)$$

In these units, the linear momentum of γ_i and γ_f are, respectively, $\vec{k}_i = E_0\hat{z}$ and $\vec{k}_f = E(\theta)\hat{n}$, where

$$\hat{n} = \cos\phi \sin\theta \hat{x} + \sin\phi \sin\theta \hat{y} + \cos\theta \hat{z},$$

and where ϕ is the azimuthal angle (refer to Fig. 1).

The spin of an incident electron in a Compton polarimeter is defined by a unit vector $\hat{S}$ relative to a system of coordinates associated with a Compton polarimeter and will be discussed in more detail in Sec. III.
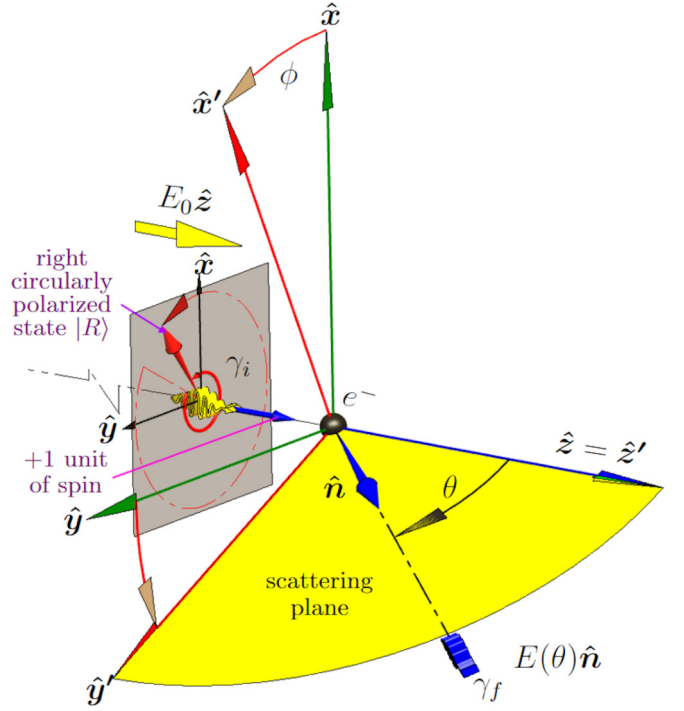

FIG. 1. Defining incident photon polarization and direction: The incident photon γ_i is characterized by its polarization state and direction, represented by the set of unit vectors $\{\hat{x}, \hat{y}, \hat{z}\}$. The photon scatters off a stationary electron at the origin, with the scatter angle θ determined by the angle between the unit vector $\hat{z}$ and the trajectory of the scattered photon γ_f defined by the unit vector $\hat{n}$. A second set of axes, $\{\hat{x}', \hat{y}', \hat{z}'\}$, is obtained by rotating anticlockwise around $\hat{z}' = \hat{z}$ by azimuthal angle ϕ. The unit vector $\hat{x}'$ is normal to the scattering plane formed by the $\hat{y}' - \hat{z}'$ unit vectors. (Scattered electron not shown.)

In this work, the scattered electron is not observed. For this reason, we do not show the scattered electrons in any figure that visually illustrates the scattering geometry. What this means in terms of calculating differential cross sections is that we have summed and averaged over the scattered electron spin.

III. DENSITY OPERATOR FOR A PAIR OF SPIN-POLARIZED ELECTRONS

Consider an incident photon in an arbitrary state of polarization denoted by $|\varphi_i\rangle$ expanded in terms of the $|R\rangle$ and $|L\rangle$ basis set such that

$$|\varphi_i\rangle = c_1|R\rangle + c_2|L\rangle, \quad (3)$$

where the probability amplitudes c_1 and c_2 are complex numbers that satisfy the normalization condition $|c_1|^2 + |c_2|^2 = 1$. The density matrix ρ_i of $|\varphi_i\rangle$ can be expressed in terms of the Stokes parameters S_{ia} ($a = 0, 1, 2, 3$) and Pauli matrices such that

$$|\varphi_i\rangle\langle\varphi_i| = \rho_i = \frac{1}{2}(S_{i0}\sigma_0 + S_{i1}\sigma_1 + S_{i2}\sigma_2 + S_{i3}\sigma_3)$$

$$= \frac{1}{2} \begin{bmatrix} S_{i0} + S_{i3} & S_{i1} - iS_{i2} \\ S_{i1} + iS_{i2} & S_{i0} - S_{i3} \end{bmatrix}, \quad (4)$$
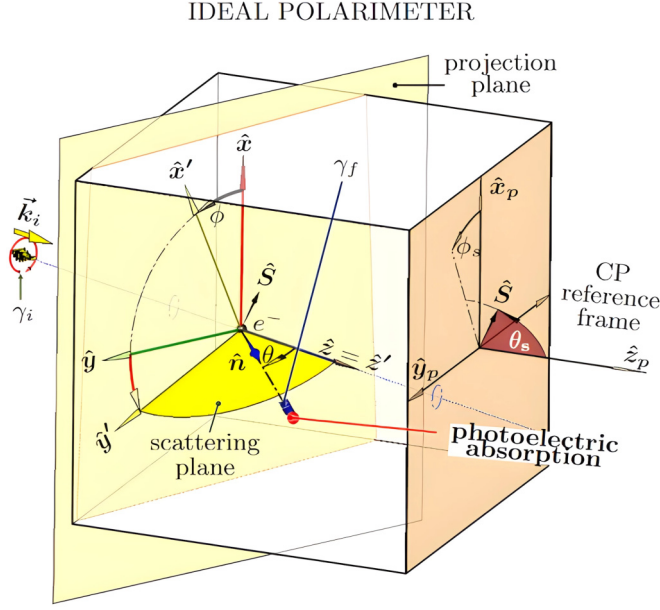
IDEAL POLARIMETER

FIG. 2. Schematic of an ideal position-sensitive Compton polarimeter (CP) that outputs coordinates of Compton scattering and scattered photoelectric absorption of the incident photon. The inclination of the scattering plane is characterized by the azimuthal angle ϕ. The incident trajectory and state of polarization are assumed to be known. The angle ϕ is obtained by the dot product $\hat{x}' \cdot \hat{x} = \cos\phi$, where the x' axis is normal to the scattering plane.

where

$$\sigma_0 = \begin{bmatrix} 1 & 0 \\ 0 & 1 \end{bmatrix}, \quad \sigma_1 = \begin{bmatrix} 0 & 1 \\ 1 & 0 \end{bmatrix}, \quad \text{and} \quad \sigma_2 = \begin{bmatrix} 0 & -i \\ i & 0 \end{bmatrix},$$

and σ_3 is given in Eq. (1a).

It is convenient to write the Stokes parameters in the form of a four-vector in this way:

$$\begin{bmatrix} S_{i0} \\ S_{i1} \\ S_{i2} \\ S_{i3} \end{bmatrix} = \begin{bmatrix} \langle\varphi_i|\sigma_0|\varphi_i\rangle \\ \langle\varphi_i|\sigma_1|\varphi_i\rangle \\ \langle\varphi_i|\sigma_2|\varphi_i\rangle \\ \langle\varphi_i|\sigma_3|\varphi_i\rangle \end{bmatrix} = \begin{bmatrix} |c_1|^2 + |c_2|^2 \\ c_1 c_2^* + c_2 c_1^* \\ i(c_1 c_2^* - c_2 c_1^*) \\ c_1 c_1^* - c_2 c_2^* \end{bmatrix}. \quad (5)$$

Figure 2 is a schematic of an ideal Compton polarimeter. The spin $\hat{S}$ of a stationary Compton electron is defined relative to a system of orthogonal coordinate axes labeled $\{x_p, y_p, z_p\}$ associated with the polarimeter itself. In this example, the plane x_p-y_p is parallel to the side of the polarimeter from which a γ_i enters the device. The spin $\hat{S}$ of the electron is defined as

$$\hat{S} = \cos\phi_s \sin\theta_s \hat{x}_p + \sin\phi_s \sin\theta_s \hat{y}_p + \cos\theta_s \hat{z}_p.$$

To determine the Compton scattering cross section of an incident photon with energy E_0 and scattered energy $E(\theta)$, we proceed by defining a density matrix ρ_e for a Compton electron, shown in Fig. 2, expressed in terms of a new set of Stokes parameters given by

$$\rho_e = \frac{1}{2}\begin{bmatrix} S_0 + S_3 & S_1 - iS_2 \\ S_1 + iS_2 & S_0 - S_3 \end{bmatrix}, \quad (6)$$

where the subscript "e" denotes electron. The Stokes parameters S_a of the Compton electron have units of $\text{cm}^2 \ \text{sr}^{-1}$ per electron, unlike the S_{ia} of the state $|\varphi_i\rangle$, which are unitless quantities.

The differential cross section can be computed via the trace operator such that

$$\frac{d\sigma}{d\Omega} = \text{Tr}(\rho_i \rho_e) \ (\text{cm}^2 \ \text{sr}^{-1} \text{ per electron}), \quad (7)$$

where the term on the left of the equal sign is the usual definition for the differential scattering cross section, and the term on the right is the trace of the matrix multiplication of the incident photon density matrix ρ_i of Eq. (4) with the density matrix of a spin-polarized Compton electron of Eq. (6). Evaluating Eq. (7) gives

$$\text{Tr}(\rho_i \rho_e) = \tfrac{1}{2}(S_{i0}S_0 + S_{i1}S_1 + S_{i2}S_2 + S_{i3}S_3). \quad (8)$$

The unknown parameters S_a are found using the Compton scattering matrix formalism [21]. The Stokes parameters in this formalism are defined in the optics representation and are labeled P_0, P_1, P_2, and P_3. The correspondence between the Stokes parameters expressed in the optical and particle physics representations are $P_0 = S_0$, $P_1 = S_1$, $P_2 = S_2$, and $P_3 = -S_3$. The appearance of the negative sign in the third parameter $P_3 = -S_3$ occurs because the helicities of circular polarization in the optical representation are opposite to the particle-physics representation.

Performing the substitution $P_{ia} \mapsto S_{ia}$ in matrix formalism prescribed by McMaster gives the following result for the Compton scattering cross section for a single photon:

$$\frac{d\sigma}{d\Omega} = \frac{r_0^2}{2}\left(\frac{E(\theta)}{E_0}\right)^2 \begin{bmatrix} 1 & 0 & 0 & 0 \end{bmatrix}$$

$$\times \begin{bmatrix} t_{11} & t_{12} & 0 & t_{14} \\ t_{12} & 2 - t_{12} & 0 & t_{24} \\ 0 & 0 & t_{33} & t_{34} \\ t_{41} & t_{42} & t_{43} & t_{44} \end{bmatrix}$$

$$\times \begin{bmatrix} 1 & 0 & 0 & 0 \\ 0 & \cos 2\phi & \sin 2\phi & 0 \\ 0 & -\sin 2\phi & \cos 2\phi & 0 \\ 0 & 0 & 0 & 1 \end{bmatrix} \begin{bmatrix} S_{i0} \\ S_{i1} \\ S_{i2} \\ -S_{i3} \end{bmatrix}, \quad (9)$$

where the interpretation of the t_{mn} matrix elements are discussed in Ref. [20]. The elements t_{mn} given in Table I can be separated into two groups: one dependent on and one independent of the spin $\hat{S}$ of a Compton electron. Evaluating Eq. (9) gives

$$\frac{d\sigma}{d\Omega} = \frac{r_0^2}{2}\left(\frac{E(\theta)}{E_0}\right)^2$$

$$\times (S_{i0}t_{11} + S_{i1}t_{12}\cos 2\phi + S_{i2}t_{12}\sin 2\phi - S_{i3}t_{14}). \quad (10)$$

Comparing Eqs. (8) and (10) term by term, one can obtain the S_a parameters for a Compton electron in terms of the t_{mn} matrix elements. Substituting in Eq. (6) gives

$$\rho_e = \frac{r_0^2}{2}\left(\frac{E(\theta)}{E_0}\right)^2 \begin{bmatrix} t_{11} - t_{14} & t_{12}e^{-2i\phi} \\ t_{12}e^{2i\phi} & t_{11} + t_{14} \end{bmatrix}. \quad (11)$$

TABLE I. Definitions of the t_{mn} matrix elements.

(a) Spin-independent terms	(b) Spin-dependent terms
$t_{11} = 1 + \cos^2\theta + [E_0 - E(\theta)](1 - \cos\theta)$	$t_{14} = -(1 - \cos\theta)[E_0\cos\theta\hat{z} + E(\theta)\hat{n}] \cdot \hat{\mathbf{S}}$
$t_{12} = t_{21} = \sin^2\theta$	$t_{24} = E_0(1 - \cos\theta)(\hat{n} \times \hat{z}) \cdot (\hat{z} \times \hat{\mathbf{S}})$
$t_{13} = t_{23} = t_{31} = t_{32} = 0$	$t_{34} = E_0(1 - \cos\theta)(\hat{z} \times \hat{n}) \cdot \hat{\mathbf{S}}$
$t_{22} = 2 - t_{12} = 2 - \sin^2\theta$	$t_{41} = -(1 - \cos\theta)[E(\theta)\cos\theta\hat{n} + E_0\hat{z}] \cdot \hat{\mathbf{S}}$
$t_{33} = 2\cos\theta$	$t_{42} = E(\theta)(1 - \cos\theta)(\hat{z} \times \hat{n}) \cdot (\hat{n} \times \hat{\mathbf{S}})$
$t_{44} = 2\cos\theta + [E_0 - E(\theta)](1 - \cos\theta)\cos\theta$	$t_{43} = -E(\theta)(1 - \cos\theta)(\hat{z} \times \hat{n}) \cdot \hat{\mathbf{S}}$

Let the density matrix $\rho_e^{(sp)}$ denote a pair of space-like separated Compton polarimeters operating in coincidence mode, where the superscript "sp" labels a pair of electron Compton polarimeters in the spin-polarized configuration. Let the density operator for electrons 1 and 2 be denoted by $\rho_e^{(1)}$ and $\rho_e^{(2)}$, respectively, such that $\rho_e^{(sp)} = \rho_e^{(1)} \otimes \rho_e^{(2)}$, or more concretely,

$$\rho_e^{(sp)} = \frac{r_0^4}{4}\left(\frac{E(\theta_1)}{E_0}\right)^2\left(\frac{E(\theta_2)}{E_0}\right)^2$$
$$\times \begin{bmatrix} (t_{11}^{(1)} - t_{14}^{(1)})(t_{11}^{(2)} - t_{14}^{(2)}) & t_{12}^{(2)}(t_{11}^{(1)} - t_{14}^{(1)})e^{-2i\phi_2} & t_{12}^{(1)}(t_{11}^{(2)} - t_{14}^{(2)})e^{-2i\phi_1} & t_{12}^{(1)}t_{12}^{(2)}e^{-2i(\phi_1+\phi_2)} \\ t_{12}^{(2)}(t_{11}^{(1)} - t_{14}^{(1)})e^{2i\phi_2} & (t_{11}^{(1)} - t_{14}^{(1)})(t_{11}^{(2)} + t_{14}^{(2)}) & t_{12}^{(1)}t_{12}^{(2)}e^{-2i(\phi_1-\phi_2)} & t_{12}^{(1)}(t_{11}^{(2)} + t_{14}^{(2)})e^{-2i\phi_1} \\ t_{12}^{(1)}(t_{11}^{(2)} - t_{14}^{(2)})e^{2i\phi_1} & t_{12}^{(1)}t_{12}^{(2)}e^{2i(\phi_1-\phi_2)} & (t_{11}^{(1)} + t_{14}^{(1)})(t_{11}^{(2)} - t_{14}^{(2)}) & t_{12}^{(2)}(t_{11}^{(1)} + t_{14}^{(1)})e^{-2i\phi_2} \\ t_{12}^{(1)}t_{12}^{(2)}e^{2i(\phi_1+\phi_2)} & t_{12}^{(1)}(t_{11}^{(2)} + t_{14}^{(2)})e^{2i\phi_1} & t_{12}^{(2)}(t_{11}^{(1)} + t_{14}^{(1)})e^{2i\phi_2} & (t_{11}^{(1)} + t_{14}^{(1)})(t_{11}^{(2)} + t_{14}^{(2)}) \end{bmatrix}, \quad (12)$$

where the superscript $l = 1, 2$ of the $t_{mn}^{(l)}$ matrix elements labels the matrix elements associated with the Compton electrons involved in the scattering of γ_1 and γ_2, respectively.

IV. PROPERTIES OF ANNIHILATION PHOTONS

Let $|\Psi_{en}\rangle$ represent the wave vector for a pair of entangled annihilation photons generated by the annihilation of an electron and a positron. Prior to their annihilation, the electron-positron pair is assumed to be momentarily bound together in a singlet state called para-positronium, often abbreviated as p-Ps. Determining $|\Psi_{en}\rangle$ requires an examination of both the physical properties of the p-Ps state itself and the conservation laws with which it must comply. In the ensuing discussion, we work in the rest frame of the p-Ps system and assume that it exists in a field-free environment. In the event of annihilation, we only consider the prevalent decay channel characterized by the emission of two maximally entangled photons.

In the rest frame of p-Ps disintegration, both photons are emitted with kinetic energy E_0 and possess identical magnitudes of linear momentum, denoted k. The net linear momentum of the emitted photons must sum to zero to conserve linear momentum. Working in a global coordinate system, if we detect photon 2 moving to the right with momentum $+\vec{k}$, then the conservation of linear momentum dictates that photon 1 must travel in the opposite direction (to the left) with momentum $-\vec{k}$. However, it is important to note that in the subsequent sections we adopt a specific nomenclature in which each photon is defined within its own local coordinate system, as depicted in Fig. 3. Consequently, we denote the momentum of photon 1 in its local coordinate system so that $\vec{k}_1 = -\vec{k}$, while the momentum of photon 2

is denoted as $\vec{k}_2 = \vec{k}$. During the initial moment of creation, the wave functions of the two photons overlap, and at this point, the two photons are identical and indistinguishable. Consequently, it is equally likely that photon 1 is emitted with momentum $+\vec{k}$ while photon 2 carries momentum $-\vec{k}$, or vice versa. This implies that the state $|\Psi_{en}\rangle$ must have two degrees of freedom in linear momenta, each with an equal probability of being observed. Thus, within the framework of the local coordinate system, two distinct momentum basis states arise: $|-k, k\rangle$ (that is, $|k_1, k_2\rangle$) and $|k, -k\rangle$ (that is, $|-k_1, -k_2\rangle$). That is, the normalized linear momentum part, denoted by $|\psi_k^{\pm}\rangle$, of the state $|\Psi_{en}\rangle$, can be described in one
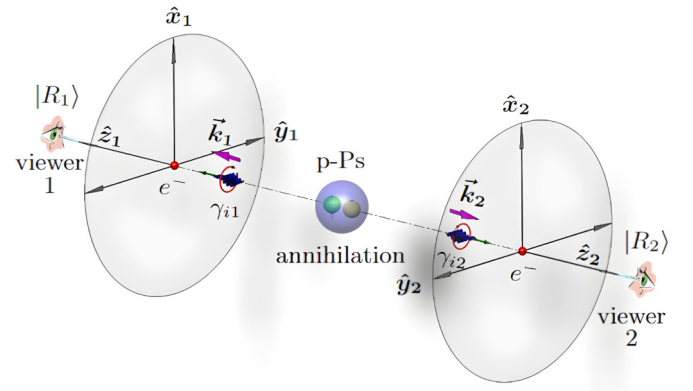

FIG. 3. In the method used here, the basis states $|R_1\rangle$ and $|R_2\rangle$ of photon 1 (γ_{i1}) and 2 (γ_{i2}), respectively, are each defined in terms of a local coordinate system represented by the set of unit vectors $\{\hat{x}_1, \hat{y}_1, \hat{z}_1\}$ and $\{\hat{x}_2, \hat{y}_2, \hat{z}_2\}$, such that $\hat{x}_1 = \hat{x}_2$, $\hat{y}_1 = -\hat{y}_2$, $\hat{z}_1 = -\hat{z}_2$, and $\vec{k}_1 = -\vec{k}_2$.

of two possible ways such that

$$|\psi_k^\pm\rangle = \frac{1}{\sqrt{2}}|k_1, k_2\rangle \pm \frac{1}{\sqrt{2}}|-k_1, -k_2\rangle, \qquad (13)$$

where the subscript "k" in $|\psi_k^\pm\rangle$ denotes the momentum state.

The singlet state of p-Ps possesses a net spin angular momentum of zero regardless of the choice of coordinate system. For the conservation of the angular momentum of the spin to hold, the spin basis vectors can only be $|R_1, R_2\rangle$ and $|L_1, L_2\rangle$. For this reason, the state $|\Psi_{en}\rangle$ must also have two degrees of freedom in spin momenta. In other words, the normalized spin angular momentum part of the state $|\Psi_{en}\rangle$ can be described in one of two possible ways. Specifically,

$$|\psi_c^\pm\rangle = \frac{1}{\sqrt{2}}|R_1, R_2\rangle \pm \frac{1}{\sqrt{2}}|L_1, L_2\rangle, \qquad (14)$$

where the subscript "c" denotes circular polarization basis. Note that both $|\psi_k^\pm\rangle$ and $|\psi_c^\pm\rangle$ represent Bell state wave vectors. This implies that the annihilation photons are maximally entangled in both linear and spin angular momenta.

Considering that the disintegration of p-Ps into two photons is an electromagnetic process, where parity is a conserved quantity, and given that p-Ps exhibit odd behavior under a parity transformation, it follows that the state $|\Psi_{en}\rangle$ must also exhibit odd behavior under such a transformation. When a parity operator $\hat{\Pi}$ is applied to the linear and angular momentum basis states, it results in the following transforms:

$$\hat{\Pi}|\pm k\rangle = |\mp k\rangle \quad \text{and} \quad \hat{\Pi}|R\rangle = |L\rangle, \quad \hat{\Pi}|L\rangle = |R\rangle.$$

For completeness, it can be shown using the definitions for $|V\rangle$, $|H\rangle$, and $|\pm 45\rangle$ in Eqs. (1b) and (1c) that

$$\hat{\Pi}|V\rangle = |V\rangle, \quad \hat{\Pi}|H\rangle = -|H\rangle, \quad \hat{\Pi}|\pm 45\rangle = \pm i|\mp 45\rangle.$$

By utilizing Eqs. (13) and (14), we can combine the even parity of the linear momentum state with the odd parity of the polarization state, and vice versa. This combination yields two potential candidates for the state $|\Psi_{en}\rangle$, both of which are normalized. Let us refer to these candidates as $|\Psi_A\rangle$ and $|\Psi_B\rangle$ such that

$$|\Psi_A\rangle = |\psi_c^-\rangle \otimes |\psi_k^+\rangle \qquad (15a)$$

and

$$|\Psi_B\rangle = |\psi_c^+\rangle \otimes |\psi_k^-\rangle. \qquad (15b)$$

Upon examining $|\Psi_A\rangle$ and $|\Psi_B\rangle$ in the given equations and referencing Eqs. (13) and (14), it becomes apparent that both states exhibit symmetry under the exchange of photons. This symmetry is expected since each state represents a configuration of two bosons.

Furthermore, it is relatively straightforward to show that both $|\Psi_A\rangle$ and $|\Psi_B\rangle$ are odd under a parity transform, and thus parity is conserved in the annihilation of p-Ps into a pair of entangled photons. That is,

$$\hat{\Pi}|\Psi_A\rangle = (-|\psi_c^-\rangle) \otimes |\psi_k^+\rangle = -|\Psi_A\rangle,$$

and

$$\hat{\Pi}|\Psi_B\rangle = |\psi_c^+\rangle \otimes (-|\psi_k^-\rangle) = -|\Psi_B\rangle.$$

Since $\langle\psi_k^-||\psi_k^+\rangle = 0$ and $\langle\psi_c^-||\psi_c^+\rangle = 0$, then $|\Psi_A\rangle$ is orthogonal to $|\Psi_B\rangle$, that is, $\langle\Psi_A||\Psi_B\rangle = 0$, implying that $|\Psi_A\rangle$ and $|\Psi_B\rangle$ represent two distinct candidates for the state $|\Psi_{en}\rangle$.

To determine which state $|\Psi_A\rangle$ or $|\Psi_B\rangle$ is the correct solution for state $|\Psi_{en}\rangle$, we direct our attention to the $|\psi_c^\pm\rangle$ states. Specifically, we expand the $|R\rangle$ and $|L\rangle$ in terms of the vertical $|V\rangle$ and $|H\rangle$ states, such that

$$|R\rangle = \frac{1}{\sqrt{2}}|V\rangle + \frac{1}{\sqrt{2}}|H\rangle,$$
$$|L\rangle = \frac{1}{\sqrt{2}}|V\rangle - \frac{1}{\sqrt{2}}|H\rangle. \qquad (16)$$

Substituting into the two solutions given in Eq. (14) gives

$$|\psi_c^-\rangle \Rightarrow \frac{1}{\sqrt{2}}|V_1, H_2\rangle + \frac{1}{\sqrt{2}}|H_1, V_2\rangle \qquad (17)$$

and

$$|\psi_c^+\rangle \Rightarrow \frac{1}{\sqrt{2}}|V_1, V_2\rangle + \frac{1}{\sqrt{2}}|H_1, H_2\rangle. \qquad (18)$$

The results of the linear polarization transformation of Eqs. (17) and (18) lead to two significant conclusions. First, the transformation from a circular to a linear polarization basis converts a Bell state into another Bell state. Second, the linear polarization transformation of $|\psi_c^-\rangle$ yields a cross-polarized Bell state. This implies that if one photon is randomly polarized in a certain plane, the other photon, traveling in the opposite direction, will be linearly polarized in a plane perpendicular to the first.

On the contrary, when the linear polarization transformation is applied to $|\psi_c^+\rangle$, it results in a coplanar polarized Bell state in which both photons are polarized in the same plane. Previous theoretical studies have demonstrated that the coincidence count rates of Compton scattering differ between photon pairs with cross- and coplanar polarization [3]. This, coupled with experimental observations which align with coincidence count rates consistent with the cross-polarized Bell state $|\psi_c^-\rangle$ [2,23–27], implies that the state $|\Psi_B\rangle$ can be excluded as a valid solution for $|\Psi_{en}\rangle$.

One other conceivable polarization state labeled as $|\phi^-\rangle$ that could serve as a potential model for describing annihilation photons is given by

$$|\phi^-\rangle = \frac{1}{\sqrt{2}}|V_1, H_2\rangle - \frac{1}{\sqrt{2}}|H_1, V_2\rangle.$$

However, upon transforming $|\phi^-\rangle$ into the circular basis, we obtain

$$|\phi^-\rangle \Rightarrow \frac{1}{\sqrt{2}}|L_1, R_2\rangle - \frac{1}{\sqrt{2}}|R_1, L_2\rangle.$$

Given that the p-Ps state has a spin of zero, upon transforming $|\phi^-\rangle$ into the circular polarization basis, it is crucial to note that the resulting state has a total spin angular momentum of two units. This observation shows that $|\phi^-\rangle$ cannot represent a viable model for entangled photons from the annihilation of p-Ps in its ground state, as it violates the conservation of the spin angular momentum.

In summary, for a state to be considered a valid candidate for annihilation photons represented by $|\Psi_{en}\rangle$, it must meet
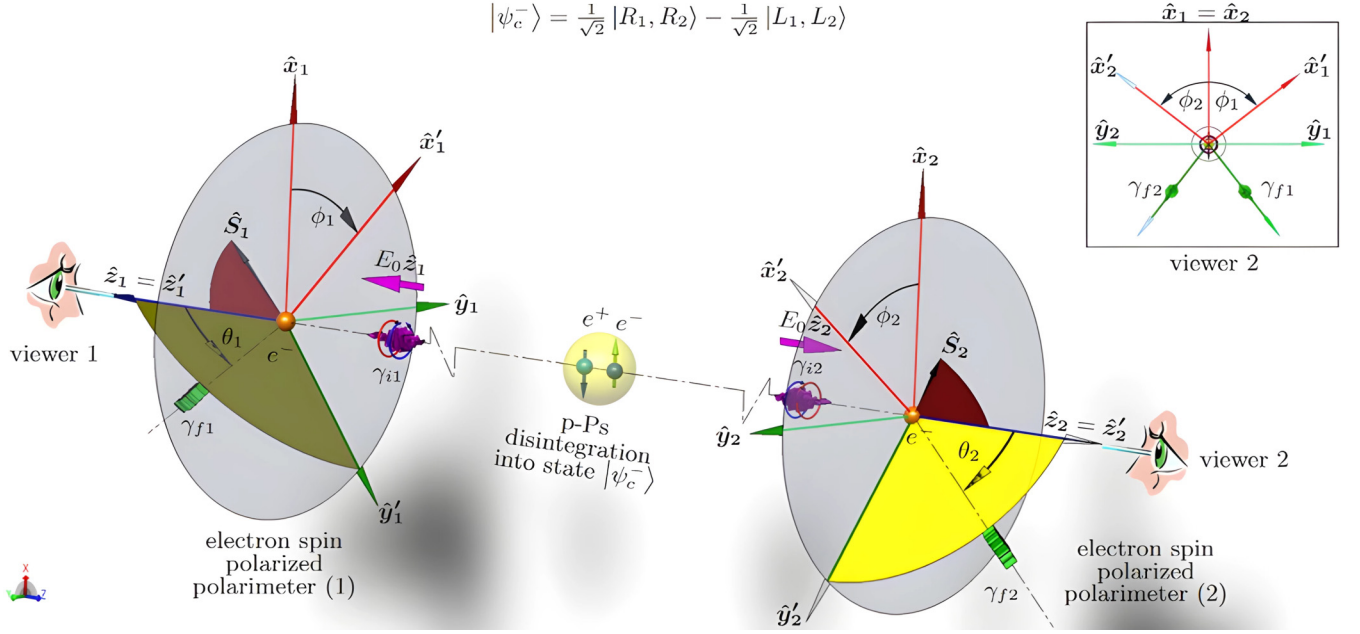
FIG. 4. Nomenclature for p-Ps entangled photons Compton scattering in the rest frame of p-Ps. Two 0.511-MeV photons, γ_1 and γ_2, move in opposite directions along a common line. Each Compton photon scatters at a polar angle θ_i ($i = 1, 2$) with a spin-polarized stationary electron. Photon states described in respective coordinate systems with the Compton electron at the origin. Insert: The perspective of viewer 2 shows the relative angle between the scattering planes as $\hat{x}'_1 \cdot \hat{x}'_2 = \cos(\phi_1 + \phi_2)$, where ϕ_1 and ϕ_2 are azimuthal angles. The trajectories of scattered photons γ_{f1} and γ_{f2} lie in the yellow shaded scattering plane, with unit vectors $\hat{x}'_1$ and $\hat{x}'_2$ perpendicular to their planes.

several requirements. First, it should exhibit rotational symmetry, ensuring the conservation of spin angular momentum (for more details, see Appendix A). Second, it must conserve parity and linear momentum. Moreover, the state should demonstrate Bose symmetry under the exchange of photons, while accounting for the indistinguishable nature of the photon pair creation. Taking these constraints into account, it is reasonable to conclude that $|\Psi_A\rangle$ satisfies all these criteria. Therefore, we can conclude that

$$|\Psi_{en}\rangle = |\Psi_A\rangle = |\psi_c^-\rangle \otimes |\psi_k^+\rangle, \quad (19a)$$

or explicitly,

$$|\Psi_{en}\rangle = \tfrac{1}{2}(|R_1, R_2\rangle - |L_1, L_2\rangle)(|k_1, k_2\rangle + |-k_1, -k_2\rangle). \quad (19b)$$

V. BASIS INDEPENDENCE

The objective of this section is to demonstrate the basis independence of the 2-Compton cross section, more commonly referred to as the Pryce-Ward joint differential cross section, for Compton scattering of annihilation photons [10]. To establish this independence, we will use the Stokes vector formalism as outlined in Refs. [21,22]. In Sec. VI, this result will be used to examine the possibility of entanglement breaking between a pair of annihilation photons through an intermediate Compton interaction.

For the purpose of the following proof, we only need to consider the polarization component $|\psi_c^-\rangle$ provided in Eq. (14), of the state vector $|\Psi_{en}\rangle$ given in Eq. (19). Thus,

$|\psi_c^-\rangle$ has the explicit form

$$|\psi_c^-\rangle = \frac{1}{\sqrt{2}}|R_1, R_2\rangle - \frac{1}{\sqrt{2}}|L_1, L_2\rangle. \quad (20)$$

In Sec. IV, it was demonstrated that the expansion of $|\psi_c^-\rangle$ in terms of the linear basis $|V\rangle$ and $|H\rangle$ results in the transformation into another Bell state, given in Eq. (17). Let $|\psi_l\rangle$ represent this transformed Bell state, with the subscript "l" indicating that it is expanded in terms of the linear basis. Specifically, we have the following:

$$|\psi_c^-\rangle \Rightarrow |\psi_l\rangle = \frac{1}{\sqrt{2}}|V_1, H_2\rangle + \frac{1}{\sqrt{2}}|H_1, V_2\rangle. \quad (21)$$

Finally, one could equally have chosen to expand $|R\rangle$ and $|L\rangle$ in terms of the diagonal basis $|+45\rangle$ and $|-45\rangle$ (refer to Appendix B), and performing the necessary calculations, we find that $|\psi_c^-\rangle$ undergoes a transformation into a Bell state represented in terms of the diagonal basis, denoted as $|\psi_d\rangle$. Here, the subscript "d" signifies the diagonal bases. Therefore, we have the following:

$$|\psi_c^-\rangle \Rightarrow |\psi_d\rangle = \frac{1}{\sqrt{2}}|+45_1, +45_2\rangle + \frac{1}{\sqrt{2}}|-45_1, -45_2\rangle. \quad (22)$$

In the above expression, it is implied that the kets $|\pm 45_1, \pm 45_2\rangle$ are cross-polarized relative to each other. To clarify, consider an example: The ket $|+45_1\rangle$ represents a plane of vibration that lies in the first and third quadrants with respect to the local coordinate system $\{x_1, y_1, z_1\}$. Similarly, the plane of vibration of $|+45_2\rangle$ lies in the first and third quadrants with respect to the local coordinate system $\{x_2, y_2, z_2\}$. However, from the perspective of the $\{x_1, y_1, z_1\}$ coordinate

system, the vibration plane of $|+45_2\rangle$ is placed in the second and fourth quadrants.

Let the density matrices corresponding to the polarization states $|\psi_c^-\rangle$, $|\psi_l\rangle$, and $|\psi_d\rangle$ be represented as $\rho_c^- = |\psi_c^-\rangle\langle\psi_c^-|$, $\rho_l = |\psi_l\rangle\langle\psi_l|$, and $\rho_d = |\psi_d\rangle\langle\psi_d|$, respectively. Since $|\psi_c^-\rangle = |\psi_l\rangle = |\psi_d\rangle$, it follows then that

$$\rho_c^- = \rho_l = \rho_d = \rho_{en} = \frac{1}{2}\begin{bmatrix} 1 & 0 & 0 & -1 \\ 0 & 0 & 0 & 0 \\ 0 & 0 & 0 & 0 \\ -1 & 0 & 0 & 1 \end{bmatrix}, \quad (23)$$

where the existence of the off-diagonal elements in the density matrix ρ_{en} is the quantum signature of an entangled superposition of product states.

The Compton scattering cross section, which describes the scattering distributions of annihilation photons in coincidence measurement using a pair of space-like separated spin polarized electrons (as depicted in Fig. 4), can now be performed by taking the trace of the matrix product between ρ_{en}, as defined in Eq. (23), and $\rho_e^{(sp)}$, Eq. (12). This can be expressed as follows:

$$\left.\frac{\partial^2\sigma}{\partial\Omega_1\partial\Omega_2}\right|_{sp} = \frac{1}{4}\mathrm{Tr}\left(\rho_{en}\rho_e^{(sp)}\right). \quad (24)$$

Expressed in terms of the matrix elements $t_{mn}^{(l)}$, Eq. (24) evaluates to

$$\left.\frac{\partial^2\sigma}{\partial\Omega_1\partial\Omega_2}\right|_{sp} = \frac{r_0^4}{16}\left(\frac{E(\theta_1)}{E_0}\right)^2\left(\frac{E(\theta_2)}{E_0}\right)^2$$
$$\times \left[t_{11}^{(1)}t_{11}^{(2)} + t_{14}^{(1)}t_{14}^{(2)} - t_{12}^{(1)}t_{12}^{(2)}\cos 2(\phi_1+\phi_2)\right]. \quad (25)$$

The term $t_{14}^{(1)}t_{14}^{(2)}$ in Eq. (25) represents the spin-spin coupling between the incoming annihilation photons and the spin-polarized Compton electrons.

For experiments using unpolarized electron spin Compton polarimeters, cross sections can be computed by setting $\hat{\mathbf{S}} = \vec{\mathbf{0}}$. In this case, the spin-dependent t_{mn} terms in Table I evaluate to zero. Let $\rho_e^{(un)}$ be a density operator that describes a pair of independent unpolarized electrons, with the subscript "*un*" indicating unpolarized electrons. Consequently, Eq. (12) simplifies to

$$\rho_e^{(un)} = \frac{r_0^4}{4}\left(\frac{E(\theta_1)}{E_0}\right)^2\left(\frac{E(\theta_2)}{E_0}\right)^2 \begin{bmatrix} t_{11}^{(1)}t_{11}^{(2)} & t_{12}^{(2)}t_{11}^{(1)}e^{-2i\phi_2} & t_{12}^{(1)}t_{11}^{(2)}e^{-2i\phi_1} & t_{12}^{(1)}t_{12}^{(2)}e^{-2i(\phi_1+\phi_2)} \\ t_{12}^{(2)}t_{11}^{(1)}e^{2i\phi_2} & t_{11}^{(1)}t_{11}^{(2)} & t_{12}^{(1)}t_{12}^{(2)}e^{-2i(\phi_1-\phi_2)} & t_{12}^{(1)}t_{11}^{(2)}e^{-2i\phi_1} \\ t_{12}^{(1)}t_{11}^{(2)}e^{2i\phi_1} & t_{12}^{(1)}t_{12}^{(2)}e^{2i(\phi_1-\phi_2)} & t_{11}^{(1)}t_{11}^{(2)} & t_{12}^{(2)}t_{11}^{(1)}e^{-2i\phi_2} \\ t_{12}^{(1)}t_{12}^{(2)}e^{2i(\phi_1+\phi_2)} & t_{12}^{(1)}t_{11}^{(2)}e^{2i\phi_1} & t_{12}^{(2)}t_{11}^{(1)}e^{2i\phi_2} & t_{11}^{(1)}t_{11}^{(2)} \end{bmatrix}. \quad (26)$$

It follows that the Compton cross section for annihilation photons scattering off unpolarized Compton electrons evaluates to

$$\left.\frac{\partial^2\sigma}{\partial\Omega_1\partial\Omega_2}\right|_{un} = \frac{r_0^4}{16}\left(\frac{E(\theta_1)}{E_0}\right)^2\left(\frac{E(\theta_2)}{E_0}\right)^2$$
$$\times \left[t_{11}^{(1)}t_{11}^{(2)} - t_{12}^{(1)}t_{12}^{(2)}\cos 2(\phi_1+\phi_2)\right]. \quad (27)$$

By substituting $E_0 = 1$ into Eq. (27), we obtain the Pryce-Ward differential cross section [10]. This finding emphasizes that the cross section described in Eq. (27), i.e., the Pryce-Ward formula itself, is not restricted to solely describing the probability of scattering of cross-polarized annihilation photons, defined in Eq. (21). Instead, it serves as a valid framework for describing the scattering probability of annihilation photons when employing the basis change defined in Eqs. (20), (21), or (22).

VI. CONTRADICTION IN ENTANGLEMENT BREAKING ASSUMPTION

When entangled particles interact with the environment, their entanglement can be lost or significantly reduced. In a recent experiment, it was reported that a complete loss of entanglement of the annihilation photons was achieved by allowing one of the annihilation photons to undergo an intermediate Compton scattering event before reaching a Compton polarimeter [12]. In these experiments, the angular correlations of the maximally entangled annihilation photons were found to be identical to those of the reported "unentangled photons." However, no conclusive evidence was provided to demonstrate the production of completely unentangled photons. In the absence of such evidence, the reported production of unentangled annihilation photons is treated as an assumption.

A change of basis in the initial annihilation photon state, as part of any valid description for an entanglement-breaking mechanism, should have no effect on the measured scattering distributions. Using the results presented in Sec. V, particularly Eq. (23), where the density matrix, denoted ρ_{en}, can be equivalently expressed in terms of the linear or circular basis ($\rho_{en} = \rho_l = \rho_c^-$), we will demonstrate that the assumed hypothesis leads to contradictory results.

The consequences of complete loss of entanglement are investigated by first considering the density matrix $\rho_{en} = \rho_l$ associated with the state vector $|\psi_l\rangle$, given in Eq. (21). In terms of the linear polarization basis, ρ_l is defined as follows:

$$\rho_{en} = \rho_l = |\psi_l\rangle\langle\psi_l| = \tfrac{1}{2}|V_1, H_2\rangle\langle V_1, H_2| + \tfrac{1}{2}|H_1, V_2\rangle\langle H_1, V_2|$$
$$+ \tfrac{1}{2}|V_1, H_2\rangle\langle H_1, V_2| + \tfrac{1}{2}|H_1, V_2\rangle\langle V_1, H_2|. \quad (28)$$

The density matrix ρ_l represents maximally entangled annihilation photons before any Compton interactions have occurred, as illustrated in Fig. 5(a). In the linear basis
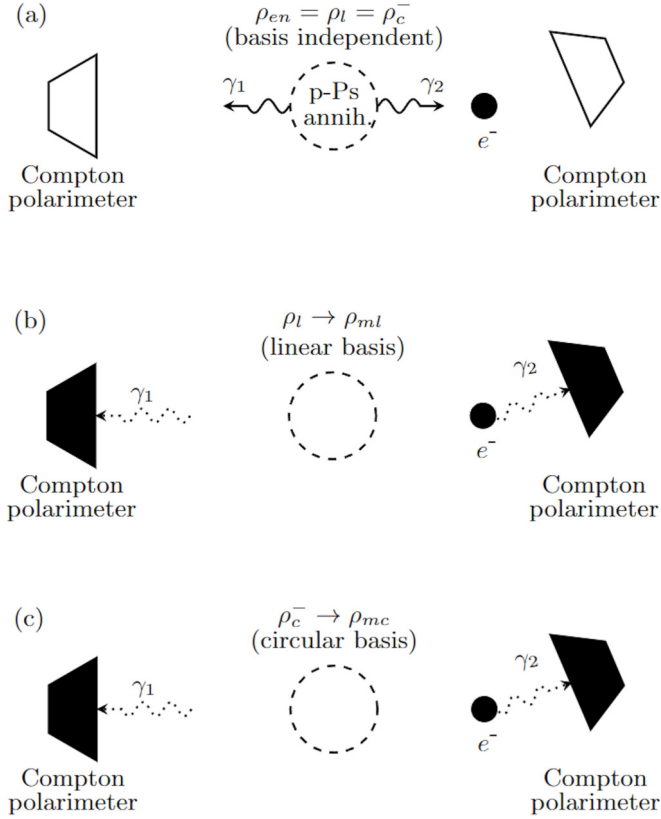
FIG. 5. Examining the consequences of the entanglement-breaking mechanism between annihilation photons (Bell state), as discussed in Ref. [12], in which the polarization correlations are preserved at small scattering angles ($<25°$). A pair of Compton polarimeters operating in coincidence mode is used to measure the scattering distributions of the resulting photons. (a) Creation of the Bell state $\rho_{en} = \rho_l = \rho_c^-$ [Eq. (23)]. (b) Considering the Bell state in the linear polarization basis, denoted by $\rho_{en} = \rho_l$, it must collapse into the mixed state ρ_{ml} [Eq. (29b)] in order to maintain the cross-polarization correlations. (c) Counterscenario: The experimental setup mirrors (b) but is considered in the circular polarization basis. To maintain the right-right or left-left polarization correlations, the state $\rho_{en} = \rho_c^-$ must collapse into the mixed state ρ_{mc} [Eq. (31b)]. Since the setups in (b) and (c) are not physically different, the assumption of entanglement breaking holds true only when the measured scattering distributions are identical.

representation, the polarization of the annihilation photons exhibits cross-polarization correlations. The assumption of complete entanglement loss holds that, to a good approximation, these cross-polarization correlations persist following Compton scattering at small angles ($<25°$). Thus, to satisfy the condition of complete entanglement loss while preserving cross-polarization correlations at small scattering angles, the third and fourth terms in Eq. (28) must vanish following the intermediate scattering, as depicted in Fig. 5(b). This results in a density matrix denoted ρ_{ml} given by

$$\rho_{ml} = \tfrac{1}{2}|V_1 H_2\rangle\langle V_1 H_2| + \tfrac{1}{2}|H_1 V_2\rangle\langle H_1 V_2|, \quad (29a)$$

where "*ml*" represents a linearly mixed cross-polarized state, which evaluates to

$$\rho_{ml} = \frac{1}{4}\begin{bmatrix} 1 & 0 & 0 & -1 \\ 0 & 1 & -1 & 0 \\ 0 & -1 & 1 & 0 \\ -1 & 0 & 0 & 1 \end{bmatrix}. \quad (29b)$$

The density matrix ρ_{ml} is the mixed state assumed to be created in an intermediate Compton scattering interaction.

However, the entangled annihilation state can be equally described in the circular basis represented by the state vector $|\psi_c^-\rangle$ [refer to Eq. (14)]. In this equivalent scenario, one could consider the entangled state in terms of the density matrix $\rho_{en} = \rho_c^-$, where

$$\begin{aligned}\rho_{en} = \rho_c^- &= |\psi_c^-\rangle\langle\psi_c^-| \\ &= \tfrac{1}{2}|R_1, R_2\rangle\langle R_1, R_2| + \tfrac{1}{2}|L_1, L_2\rangle\langle L_1, L_2| \\ &\quad - \tfrac{1}{2}|R_1, R_2\rangle\langle L_1, L_2| - \tfrac{1}{2}|L_1, L_2\rangle\langle R_1, R_2|, \quad (30)\end{aligned}$$

In the circular basis representation, the polarization of the annihilation photons exhibits right-right and left-left polarization correlations. If we again invoke the same assumption that the polarization correlations persist following Compton scattering at small angles, as depicted in Fig. 5(c), then the third and fourth terms in Eq. (30) must also vanish after the intermediate scattering event. This leads to a density matrix denoted by ρ_{mc}, such that

$$\rho_{mc} = \tfrac{1}{2}|R_1, R_2\rangle\langle R_1, R_2| + \tfrac{1}{2}|L_1, L_2\rangle\langle L_1, L_2|, \quad (31a)$$

which evaluates to

$$\rho_{mc} = \frac{1}{2}\begin{bmatrix} 1 & 0 & 0 & 0 \\ 0 & 0 & 0 & 0 \\ 0 & 0 & 0 & 0 \\ 0 & 0 & 0 & 1 \end{bmatrix}. \quad (31b)$$

If the states ρ_{ml} or ρ_{mc} are then measured using a pair of Compton polarimeters in coincidence mode, as depicted in Figs. 5(b) and 5(c), then the cross sections for ρ_{ml} and ρ_{mc} can be evaluated, respectively, as follows:

$$\begin{aligned}\frac{1}{4}\mathrm{Tr}(\rho_{ml}\rho^{(un)}) &= \frac{r_0^4}{16}\left(\frac{E(\theta_1)}{E_0}\right)^2\left(\frac{E(\theta_2)}{E_{02}}\right)^2 \\ &\quad \times \left(t_{11}^{(1)}t_{11}^{(2)} - t_{12}^{(1)}t_{12}^{(2)}\cos 2\phi_1\cos 2\phi_2\right)\end{aligned}$$
$$(32a)$$

and

$$\frac{1}{4}\mathrm{Tr}\left(\rho_{mc}\rho_e^{(un)}\right) = \frac{r_0^4}{16}\left(\frac{E(\theta_1)}{E_0}\right)^2\left(\frac{E(\theta_2)}{E_{02}}\right)^2 t_{11}^{(1)}t_{11}^{(2)}, \quad (32b)$$

where E_{02} is the incident energy of γ_2 as it enters the polarimeter on the right in Figs. 5(b) and 5(c) such that $E_{02} < E_0$.

Upon examination of Eqs. (32a) and (32b), it becomes evident that, in general, the proposed assumption of complete entanglement breaking leads to nonequivalent cross sections. Only for specific values of $\phi_1 = \phi_2 = \pm\pi/4, \pm 3\pi/4$ will the assumption of breaking the entanglement, as stipulated, not lead to contradictory experimental results. Therefore, this qualitative line of reasoning, involving a change in basis, demonstrates that a single intermediate Compton scattering

event cannot, in general, completely break entanglement in the manner adopted by the assumption, as it would lead to paradoxical experimental outcomes. Consequently, conclusions based on this proposition would require a reinterpretation.

VII. CLASSICAL VS QUANTUM CORRELATIONS

This section aims to address the conflicting reports [28–32] concerning the predicted azimuthal correlations of the mixed state ρ_{ml}.

To quantify the azimuthal correlations between pairs of photons in Compton scattering experiments, we consider the case where both θ_1 and θ_2 are equal to a common value θ. By comparing the counting rate $N_\perp$ when the sum of the azimuthal angles ϕ_1 and ϕ_2 is $90°$ with the counting rate $N_\parallel$ when the sum is $0°$, we can calculate the asymmetric ratio

$$Z(\theta) = \frac{N_\perp}{N_\parallel}. \tag{33}$$

The functions of the asymmetric ratios Z_{en} and Z_{ml} are defined in terms of the t_{mn} matrix elements. These functions can be obtained using the Compton cross sections for ρ_{en} [Eq. (27)] and ρ_{ml} [Eq. (32a)], such that

$$Z(\theta)_{en} = \frac{t_{11}^2 + t_{12}^2}{t_{11}^2 - t_{12}^2} \tag{34a}$$

(refer to Appendix E) and

$$Z(\theta, \phi_2)_{ml} = \frac{t_{11}^2 + t_{12}^2 \cos^2 2\phi_2}{t_{11}^2 - t_{12}^2 \cos^2 2\phi_2} \tag{34b}$$

(refer to Appendix F).

This analysis shows that the asymmetric ratio $Z(\theta, \phi_2)_{ml}$ has a value of 1 for any scattering angle θ only when ϕ_2 has values of $\pm\pi/4, \pm 3\pi/4$, which is different from the reported result in Refs. [28,33], where it is claimed that $Z(\theta, \phi_2)_{ml}$ is unity for all values of θ and azimuthal angles.

Upon further examination of the asymmetric ratios given in Eq. (34), we find that the ratio for the annihilation photons, as described by Eq. (34a), remains invariant with respect to the azimuthal angle. However, setting $\phi_2 = 0$ in Eq. (34b) results in $Z(\theta)_{en} = Z(\theta, \phi_2 = 0)_{ml}$.

Indeed, setting $\phi_2 = 0$ in the cross sections for ρ_{en} [Eq. (27)] and ρ_{ml} [Eq. (32a)], we obtain the following identity:

$$\frac{\partial^2 \sigma(\phi_2 = 0)}{\partial \Omega_1 \partial \Omega_2}\bigg|_{ml} = \frac{\partial^2 \sigma(\phi_2 = 0)}{\partial \Omega_1 \partial \Omega_2}\bigg|_{unp} = \frac{r_0^4}{16}\left(\frac{E(\theta_1)}{E_0}\right)^2$$
$$\times \left(\frac{E(\theta_2)}{E_0}\right)^2 \left(t_{11}^{(1)} t_{11}^{(2)} - t_{12}^{(1)} t_{12}^{(2)} \cos 2\phi_1\right). \tag{35}$$

This situation for the mixed state ρ_{ml} is depicted diagrammatically in Fig. 6.

Hiesmayr *et al.* [3] also observed a similar identity using Kraus-type structures to calculate Compton scattering cross sections. However, it is important to note that this identity does not require mutually unbiased bases to distinguish between states ρ_{ml} and ρ_{en}. The reason for this lies in the
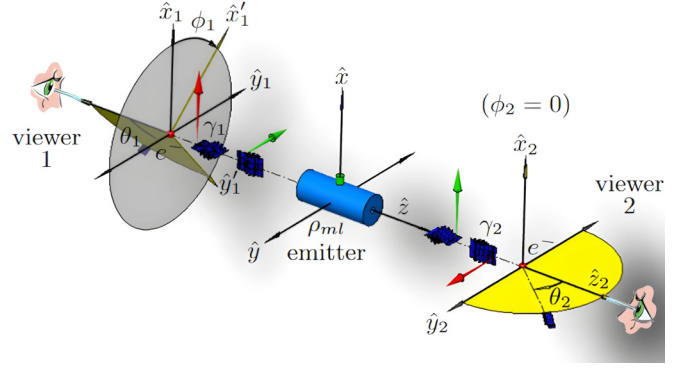

FIG. 6. The scenario where the Compton cross section for the ρ_{ml} mixed state matches that of maximally entangled annihilation photons represented by the density matrix ρ_{en}. A hypothetical mixed-state photon emitter releases 0.511-MeV photon pairs, each undergoing subsequent Compton scattering. In the case ρ_{ml}, the photon polarization is exclusively aligned along the x or y axis. The counting rates depend on the chosen coordinate system relative to the direction of polarization. To achieve identical coincidence rates as annihilation photons, the x and y axes of a local coordinate system must align with the states $|V\rangle$ and $|H\rangle$ of the emitted pair. To achieve this, we set $\phi_2 = 0$ and allow γ_1 to scatter at any (θ_1, ϕ_1). In contrast to annihilation photons, the counting rate remains invariant under a rotation about the propagation axis.

conservation of the spin angular momentum during the disintegration of p-Ps, which prevents the production of ρ_{ml} with polarization states exclusively aligned along the x axis or the y axis. In contrast, ρ_{en} (detailed in Appendix A) is rotationally symmetric about the propagation axis.

VIII. WITNESSING ENTANGLEMENT IN ANNIHILATION PHOTONS

In the previous section, it was demonstrated that the asymmetric ratio of the state ρ_{ml} lacks rotational invariance around the axes of propagation, unlike the ratio for annihilation photons denoted as ρ_{en}. This invariance is a consequence of the state ρ_{ml} no longer representing, as it did in the original system of coordinates, a state in which the two photons have orthogonal directions of polarization. Instead, it can be shown that, in a rotated frame, these directions can be orthogonal or parallel.

Bohm and Aharonov [34] showed that the correct wave function for the annihilation photons must ensure that the polarization of the two photons maintains orthogonality, regardless of the chosen x-y axes. To allow for this symmetry in a classical model of the annihilation photons, where the quantum superposition principle is not present, they supposed that when the annihilation photons are created and each photon has separated sufficiently from the other, the annihilation photons are no longer described by the wave function $|\psi_l\rangle$, Eq. (21), which has a definite phase relation between its components. Instead, they considered a classically cross-polarized correlated mixed state $\rho(\alpha)_l$ (refer to Appendix C for more details)

given by

$$\rho(\alpha)_l = \tfrac{1}{2}|V_1(-\alpha), H_2(\alpha)\rangle\langle V_1(-\alpha), H_2(\alpha)|$$
$$+ \tfrac{1}{2}|H_1(-\alpha), V_2(\alpha)\rangle\langle H_1(-\alpha), V_2(\alpha)|. \quad (36)$$

Relative to a rotated frame about the propagation axis by an angle α, each photon of the cross-polarized mixed state $\rho(\alpha)_l$ has some definite state of linear polarization, which is at right angles to that of the other. To obtain symmetry in the final statistical results, they supposed, wherever necessary, that there is a uniform statistical distribution over any direction that may be favored in each individual case.

Let the density matrix ρ_{ls} denote this supposed mixed state. This state can be obtained by taking the sum of the individual cases denoted by $\rho(\alpha)_l$, where the azimuthal angle α ranges from 0 to 2π, weighted by a probability of $1/2\pi$ for each angle α, such that

$$\rho_{ls} = \frac{1}{2\pi}\int_{\alpha=0}^{2\pi}\rho(\alpha)_{lr}d\alpha = \frac{1}{4}\begin{bmatrix} 1 & 0 & 0 & -1 \\ 0 & 1 & 0 & 0 \\ 0 & 0 & 1 & 0 \\ -1 & 0 & 0 & 1 \end{bmatrix}, \quad (37)$$

where the subscript "s" refers to a rotationally symmetric cross-polarized mixed state.

In many cases, one obtains the same probability for an arbitrary direction of polarization of any one of the photons. While $\rho(\alpha)_l$ itself does not maintain a net spin of zero under rotation around the propagation axis, on average, the conservation of angular momentum holds for ρ_{ls} (for more details, see Appendix D).

The cross section for ρ_{ls} is given by

$$\frac{1}{4}\mathrm{Tr}\big(\rho_{ls}\rho_e^{(un)}\big) = \frac{r_0^4}{32}\left(\frac{E(\theta_1)}{E_0}\right)^2\left(\frac{E(\theta_2)}{E_0}\right)^2$$
$$\times\big[2t_{11}^{(1)}t_{11}^{(2)} - t_{12}^{(1)}t_{12}^{(2)}\cos 2(\phi_1+\phi_2)\big]. \quad (38)$$

The corresponding asymmetric ratio $Z(\theta)_{ls}$ of ρ_{ls} is given by (see Appendix G for more detail)

$$Z(\theta)_{ls} = \frac{2t_{11}^2 + t_{12}^2}{2t_{11}^2 - t_{12}^2}. \quad (39)$$

As can be seen, Eq. (39) is invariant under a rotation about the propagation axis. The density matrix ρ_{ls} serves as a sufficient classical counterpart of the entangled state ρ_{en} since it maintains similar polarization correlations and symmetrical properties of the wave function given in Eq. (21) of the entangled annihilation photon. Figure 7 plots the asymmetric ratio for both the maximally entangled state ρ_{en} and its classical counterpart ρ_{ls}.

The analytical solution for the ratio of ρ_{ls} is compared to the QE-GEANT4 simulation of the same state provided by Watts *et al.* [2]. The simulated and theoretical results for the mixed state ρ_{ls} agree well. Furthermore, the upper bound of the mixed state ρ_{ls}, found to be 1.63, aligns with the result reported in Ref. [34]. The asymmetric ratio of the mixed state ρ_{ls} serves as an upper bound that delineates between azimuthal correlations influenced by entanglement and those not. Any experimental data falling within the shaded yellow region signifies azimuthal correlations influenced by entanglement.
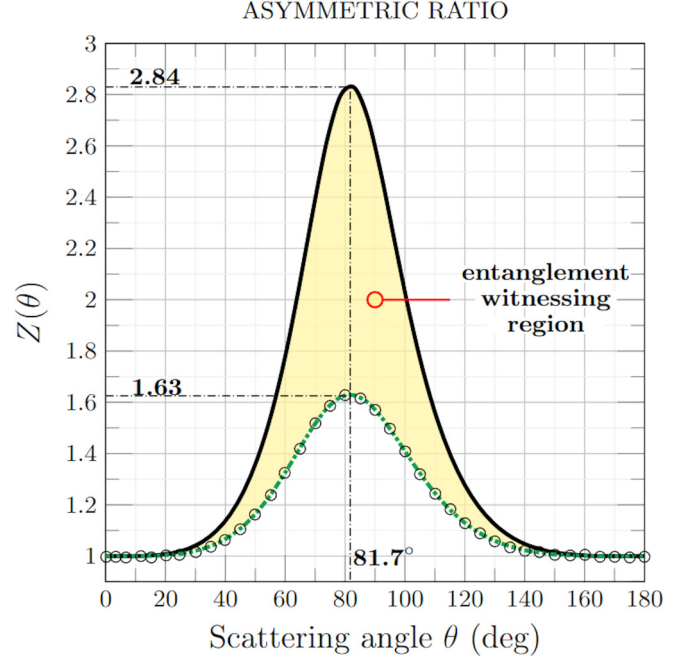

FIG. 7. Entanglement witnessing (shaded region) for annihilation photons in asymmetric ratio-type measurements, as a function of the Compton scattering angle $\theta_1 = \theta_2 = \theta$ for the ideal geometry. The annihilation state (–), Eq. (34a), is compared to its classical counterpart ρ_{sl} (–), Eq. (39). QE-GEANT4 generated results for state ρ_{sl} (°) by Watts *et al.* [2].

An alternative approach to witnessing entanglement in annihilation photons is through a quantity $R(\theta, \eta)$. It is defined as

$$R(\theta, \eta) = 1 + \frac{1 - Z(\theta)}{1 + Z(\theta)}\cos 2\eta, \quad (40)$$

where $\eta = \phi_1 + \phi_2$. The quantity $R(\theta, \eta)$ has several useful properties. Firstly, deviations of $R(\theta, \eta)$ from unity indicate correlations between the momenta [24]. When the momenta of the scattered photons are uncorrelated, $R(\theta, \eta)$ equals unity for all values of η. Lastly, to discern between azimuthal correlations influenced by entanglement and those that are not, a modified function denoted by $\mathcal{R}(\theta, \eta)$ can be obtained by changing $R(\theta, \eta)$ so that the minimum value of $\mathcal{R}(\theta, \eta)$ is unity. For an ideal geometry with $\theta_1 = \theta_2 = \theta = 81.7°$, we can evaluate $\mathcal{R}(\theta, \eta)$ for states ρ_{en} and ρ_{sl} as

$$\mathcal{R}(\theta = 81.7°, \eta)_{en} = 1.479 - 0.479\cos 2\eta \quad (41a)$$

and

$$\mathcal{R}(\theta = 81.7°, \eta)_{ls} = 1.240 - 0.240\cos 2\eta. \quad (41b)$$

For a detailed derivation of Eqs. (41a) and (41b), please refer to Appendixes F and G, respectively.

The plots of $\mathcal{R}(\theta, \eta)_{en}$ and $\mathcal{R}(\theta, \eta)_{ls}$ are presented in Fig. 8. The function $\mathcal{R}(\theta, \eta)_{ls}$ serves as an upper bound for classically induced correlations. Data points above this bound indicate correlations influenced by entanglement.
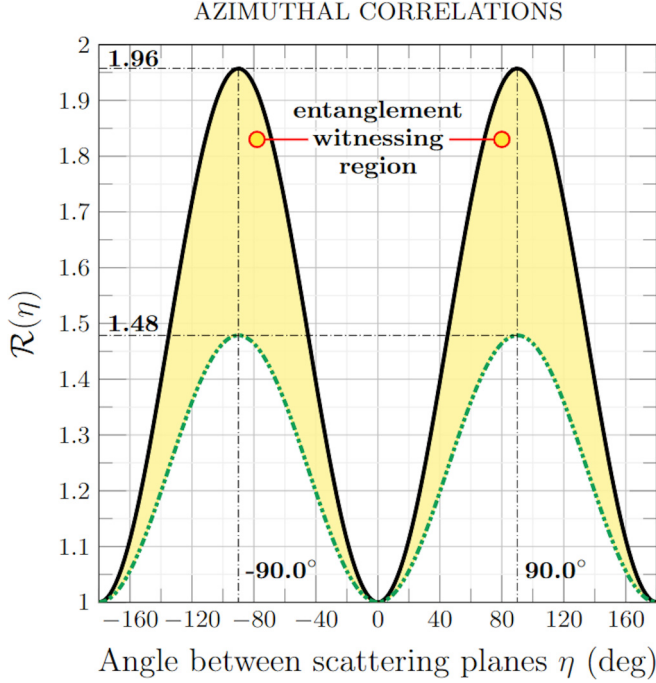
AZIMUTHAL CORRELATIONS

FIG. 8. Entanglement witnessing (shaded region) for annihilation photons as a function of the angle $\eta = \phi_1 + \phi_2$ between the scattering planes in the case of an ideal geometry and where ($\theta_1 = \theta_2 = \theta = 81.7°$). Annihilation photons (–), Eq. (41a), and their classical counterparts (–), Eq. (41b).

IX. CONCLUSION

We have developed a flexible theoretical framework that serves as the foundation for a scalable program encompassing the multiple scattering of spin-polarized and unpolarized electrons, that can be also applied to various interaction types. Our investigation reveals that the Compton cross section for annihilation photons remains independent of the photon polarization basis. This finding leads us to present a qualitative argument demonstrating that a single Compton scattering event does not necessarily result in complete entanglement breaking between annihilation photons.

Furthermore, we demonstrate that there is no need to invoke the contemporary theoretical requirement of mutually unbiased bases to conduct unambiguous entanglement-witnessing measurements on annihilation photons. Instead, a comparison with a hypothetical classical counterpart is sufficient to distinguish between azimuthal correlations influenced by entanglement and those unaffected by it.

As part of our program, we will incorporate theory to advance QE-GEANT4, enabling it to account for the behavior of entangled photons involved in multiple scattering events, and a theoretical description is currently being developed to quantify the degree of entanglement in Compton interactions. Indeed, the use of principles derived from x-ray quantum optics in the MeV wavelength range shows substantial potential for advancements in various domains, including quantum-enhanced detection [35], quantum cryptography [36], ghost imaging, quantum lithography [37], and the facilitation of quantum coherence, as well as enabling quantum teleportation over extensive interstellar distances [38,39]. The successful

measurement of pairs of x-ray photons with minimal background noise serves as evidence of the feasibility of observing quantum optic phenomena using x-ray photons [37]. Consequently, we anticipate that the framework outlined in this paper will provide a basis for evaluating the practicality of extending quantum optics into the MeV energy regime.

APPENDIX A: ROTATIONAL SYMMETRY OF ANNIHILATION PHOTONS

Rotating the x-y coordinate axes by an angle β is equivalent to applying the matrix $M(\beta)$ to a Jones vector [40] such that

$$M(\beta) = \begin{bmatrix} e^{i\beta} & 0 \\ 0 & e^{-i\beta} \end{bmatrix}. \tag{A1}$$

For state $|\psi_c^-\rangle$, Eq. (20), to conserve spin angular momentum, it must be rotationally invariant under rotation of the z axis. This article describes the quantum state of photons 1 and 2 in relation to local coordinate systems defined by the set of axes $\{x_1, y_1, z_1\}$ and $\{x_2, y_2, z_2\}$, respectively. If viewer 2 applies a counterclockwise rotation of the axes by an angle β about the z_2 axis, then viewer 1 must apply a clockwise rotation by $-\beta$ about the z_1 axis, ensuring that both local coordinate systems rotate in unison. Under this rotation, the state transforms into

$$|\psi_c^-\rangle \Longrightarrow |\psi_c^-(\beta)\rangle = M(-\beta) \otimes M(\beta)|\psi_c^-\rangle, \tag{A2}$$

which implies that

$$|\psi_c^-(\beta)\rangle = \frac{1}{\sqrt{2}}M(-\beta)|R_1\rangle \otimes M(\beta)|R_2\rangle$$
$$- \frac{1}{\sqrt{2}}M(-\beta)|L_1\rangle \otimes M(\beta)|L_2\rangle. \tag{A3}$$

Evaluating gives

$$|\psi_c^-(\beta)\rangle = \frac{1}{\sqrt{2}}e^{-i\beta}|R_1\rangle \otimes e^{i\beta}|R_2\rangle$$
$$- \frac{1}{\sqrt{2}}e^{i\beta}|L_1\rangle \otimes e^{-i\beta}|L_2\rangle. \tag{A4}$$

Since $e^{\pm i\beta}$ are pure phases and $e^{-i\beta}e^{i\beta} = 1$, then it follows that

$$|\psi_c^-(\beta)\rangle = |\psi_c^-\rangle. \tag{A5}$$

Therefore, this implies that the density operator ρ_{en} of $|\psi_c^-\rangle$ is also invariant under a rotation of the coordinate system, such that

$$|\psi_c^-(\beta)\rangle\langle\psi_c(\beta)| = |\psi_c^-\rangle\langle\psi_c^-|. \tag{A6}$$

APPENDIX B: CHANGE OF BASIS

The expansion of $|R\rangle$ and $|L\rangle$ basis in terms of the diagonal basis $|\pm 45\rangle$ is given by

$$|R\rangle = \frac{1}{\sqrt{2}}|+45\rangle + \frac{1}{\sqrt{2}}|-45\rangle,$$

$$|L\rangle = \frac{i}{\sqrt{2}}|-45\rangle - \frac{i}{\sqrt{2}}|+45\rangle. \tag{B1}$$

APPENDIX C: BASIS ROTATION

If the SU(2) matrix $M(\alpha)$ in Eq. (A1) represents a rotation of a local coordinate system around the z axis by an angle α, then $M(\alpha)^\dagger$ represents a rotation of a Jones vector about the z axis by an angle α. To clearly differentiate between the rotation of a coordinate system and the rotation of a Jones vector, we introduce a rotation matrix $N(\alpha)$, where

$$M(\alpha)^\dagger = N(\alpha) = \begin{bmatrix} e^{-i\alpha} & 0 \\ 0 & e^{i\alpha} \end{bmatrix}. \tag{C1}$$

The rotation of the vertical $|V\rangle$ and horizontal $|H\rangle$ basis, given in Eq. (1b), with respect to the local coordinate systems labeled 1 and 2, can be expressed as follows:

$$N(-\alpha)|V\rangle = |V_1(-\alpha)\rangle = \frac{1}{\sqrt{2}}\begin{bmatrix} e^{i\alpha} \\ e^{-i\alpha} \end{bmatrix},$$

$$N(-\alpha)|H\rangle = |H_1(-\alpha)\rangle = \frac{1}{\sqrt{2}}\begin{bmatrix} e^{i\alpha} \\ -e^{-i\alpha} \end{bmatrix}, \tag{C2a}$$

and

$$|V_2(\alpha)\rangle = N(\alpha)|V\rangle = \frac{1}{\sqrt{2}}\begin{bmatrix} e^{-i\alpha} \\ e^{i\alpha} \end{bmatrix},$$

$$|H_2(\alpha)\rangle = N(\alpha)|H\rangle = \frac{1}{\sqrt{2}}\begin{bmatrix} e^{-i\alpha} \\ -e^{i\alpha} \end{bmatrix}. \tag{C2b}$$

APPENDIX D: ROTATIONAL SYMMETRY OF STATE ρ_{sl}

Using the SU(2) matrix $M(\alpha)$ in Eq. (A1), we can rotate around the z axis with respect to the mixed state ρ_{ls} given in Eq. (37). This rotation yields the density matrix in the rotated frame, denoted as $\rho(\beta)_{ls}$, which can be expressed as

$$\rho(\beta)_{ls} = M(-\beta) \otimes M(\beta)\rho_{ls}[M(-\beta) \otimes M(\beta)]^\dagger. \tag{D1}$$

Evaluating the above equation, it can be shown that

$$\rho_{ls}(\beta) = \rho_{ls}. \tag{D2}$$

Hence, it follows that ρ_{ls} exhibits rotational symmetry.

APPENDIX E: ASYMMETRIC RATIO AND AZIMUTHAL CORRELATION FUNCTIONS OF ρ_{en}

By utilizing the cross section presented in Sec. V, Eq. (27), which characterizes the Compton scattering of the state ρ_{en} of annihilation photons, we define the function

$$F(\theta, \eta)_{en} = t_{11}^2 - t_{12}^2 \cos 2\eta, \tag{E1}$$

where we have set $\theta_1 = \theta_2 = \theta$ and $\eta = \phi_1 + \phi_2$.

The theoretical counting rate for $\eta = \pi/2$ is proportional to the function denoted as $F(\theta)_{en}^{(\perp)}$ such that

$$F(\theta)_{en}^{(\perp)} = t_{11}^2 + t_{12}^2. \tag{E2a}$$

The theoretical counting rate for $\eta = 0°$ is proportional to the function denoted as $F(\theta)_{en}^{(\|)}$ such that

$$F(\theta)_{en}^{(\|)} = t_{11}^2 - t_{12}^2. \tag{E2b}$$

Hence, the asymmetric ratio $Z(\theta)_{en}$ for annihilation photons is given by

$$Z(\theta)_{en} = \frac{t_{11}^2 + t_{12}^2}{t_{11}^2 - t_{12}^2} \quad \text{Q.E.D.} \tag{E3}$$

The associated azimuthal correlation function $R(\theta, \eta)_{en}$ is given by

$$R(\theta, \eta)_{en} = \frac{F(\theta, \eta)_{en}}{t_{11}^2} = 1 - \frac{t_{12}^2}{t_{11}^2} \cos 2\eta. \tag{E4}$$

Using Eq. (E3), we can show that

$$\frac{t_{12}^2}{t_{11}^2} = -\frac{1 - Z(\theta)_{en}}{1 + Z(\theta)_{en}}. \tag{E5}$$

Substituting Eq. (E5) into Eq. (E4) gives

$$R(\theta, \eta)_{en} = 1 + \frac{1 - Z(\theta)_{en}}{1 + Z(\theta)_{en}} \cos 2\eta \quad \text{Q.E.D.} \tag{E6}$$

We analyze the azimuthal correlation function at the scattering angle of 81.7°. The minimum of $R(\theta, \eta)_{en}$ occurs at $\eta = 0$, so that $R(81.7°, 0) = 0.521$. Therefore, the shifted function $\mathcal{R}(\eta)_{en}$ is given by

$$\mathcal{R}(\eta)_{en} = R(81.7°, \eta)_{en} + (1 - 0.5214), \tag{E7}$$

which evaluates to

$$\mathcal{R}(\eta)_{en} = 1.479 - 0.479 \cos 2\eta \quad \text{Q.E.D.} \tag{E8}$$

APPENDIX F: ASYMMETRIC RATIO AND AZIMUTHAL CORRELATION FUNCTIONS OF ρ_{ml}

Utilizing the cross section presented in Sec. VII, Eq. (35), which characterizes the Compton scattering of the mixed cross polarized state ρ_{ml}, we define the function

$$F(\theta, \eta)_{ml} = t_{11}^2 - t_{12}^2 \cos 2\phi_1 \cos 2\phi_2, \tag{F1}$$

where we have set $\theta_1 = \theta_2 = \theta$.

The theoretical counting rate for $\phi_1 + \phi_2 = \pi/2$ is obtained by substituting $\phi_1 = \pi/2 - \phi_2$ into Eq. (F1) and is proportional to the function denoted as $F(\theta)_{ml}^{(\perp)}$ such that

$$F(\theta)_{ml}^{(\perp)} = t_{11}^2 + t_{12}^2 \cos^2 2\phi_2. \tag{F2a}$$

The theoretical counting rate for $\phi_1 + \phi_2 = 0$ is obtained by substituting $\phi_1 = -\phi_2$ into Eq. (F1), and is proportional to the function denoted as $F(\theta)_{ml}^{(\|)}$ such that

$$F(\theta)_{ml}^{(\|)} = t_{11}^2 - t_{12}^2 \cos^2 2\phi_2. \tag{F2b}$$

Hence, the asymmetric ratio $Z(\theta)_{ml}$ is given by

$$Z(\theta)_{ml} = \frac{t_{11}^2 + t_{12}^2 \cos^2 2\phi_2}{t_{11}^2 - t_{12}^2 \cos^2 2\phi_2} \quad \text{Q.E.D.} \tag{F3}$$

APPENDIX G: ASYMMETRIC RATIO AND AZIMUTHAL CORRELATION FUNCTIONS OF ρ_{ls}

By employing a similar line of reasoning as described in Appendix E, we can deduce the asymmetrical ratio $Z(\theta)_{sl}$ for the mixed state ρ_{sl} given in Sec. VIII [Eq. (37)]. This mixed state, when subjected to Compton scattering, is governed by the cross section given in Eq. (38). We define the function

$$F(\theta, \eta)_{ls} = 2t_{11}^2 - t_{11}^2 \cos 2\eta, \tag{G1}$$

where we have set $\theta_1 = \theta_2 = \theta$ and $\eta = \phi_1 + \phi_2$.

The theoretical counting rate for $\eta = \pi/2$ is proportional to the function denoted as $F(\theta)_{ls}^{(\perp)}$ such that

$$F(\theta)_{ls}^{(\perp)} = 2t_{11}^2 + t_{12}^2. \tag{G2a}$$

The theoretical counting rate for $\eta = 0°$ is proportional to the function denoted as $F(\theta)_{ls}^{(\|)}$ such that

$$F(\theta)_{ls}^{(\|)} = 2t_{11}^2 - t_{12}^2. \tag{G2b}$$

Hence, the asymmetric ratio $Z(\theta)_{ls}$ is given by

$$Z(\theta)_{ls} = \frac{2t_{11}^2 + t_{12}^2}{2t_{11}^2 - t_{12}^2} \quad \text{Q.E.D.} \tag{G3}$$

The associated azimuthal correlation function $R(\theta, \eta)_{ls}$ is given by

$$R(\theta, \eta)_{ls} = 1 + \frac{1 - Z(\theta)_{ls}}{1 + Z(\theta)_{ls}} \cos 2\eta. \tag{G4}$$

We analyze the azimuthal correlation function at the scattering angle of $81.7°$ and find that the minimum value of $R(\theta = 81.7°, \eta = 0°)_{ls}$ is equal to 0.761. Hence,

$$\mathcal{R}(\eta)_{ls} = R(\theta, \eta)_{ls} + (1 - 0.761). \tag{G5}$$

Upon evaluation, we obtain

$$\mathcal{R}(\eta)_{ls} = 1.240 - 0.240 \cos 2\eta \quad \text{Q.E.D.} \tag{G6}$$

[1] V. D. Irby, Phys. Rev. A **67**, 034102 (2003).

[2] D. P. Watts, J. Bordes, J. R. Brown, A. Cherlin, R. Newton, J. Allison, M. Bashkanov, N. Efthimiou, and N. A. Zachariou, Nat. Commun. **12**, 2646 (2021).

[3] B. C. Hiesmayr and P. Moskal, Sci. Rep. **9**, 8166 (2019).

[4] Y. Ma, J. Hua, D. Liu, Y. He, T. Zhang, J. Chen, F. Yang, X. Ning, H. Zhang, Y. Du, and W. Lu, Phys. Rev. Appl. **19**, 014073 (2023).

[5] N. Numadate, S. Oishi, H. Odaka, Priti, M. Sakurai, T. Takahashi, Y. Tsuzuki, Y. Uchida, H. Watanabe, S. Watanabe, H. Yoneda, and N. Nakamura, Phys. Rev. A **105**, 023109 (2022).

[6] M. Vockert, G. Weber, H. Bräuning, A. Surzhykov, C. Brandau, S. Fritzsche, S. Geyer, S. Hagmann, S. Hess, C. Kozhuharov, R. Märtin, N. Petridis, R. Hess, S. Trotsenko, Y. A. Litvinov, J. Glorius, A. Gumberidze, M. Steck, S. Litvinov, T. Gaßner *et al.*, Phys. Rev. A **99**, 052702 (2019).

[7] Y. Du, Z. He, G. Knoll, D. Wehe, and W. Li, Nucl. Instrum. Methods Phys. Res. Sect. A **457**, 203 (2001).

[8] G. Yabu, H. Yoneda, T. Orita, S. Takeda, P. Caradonna, T. Takahashi, S. Watanabe, and F. Moriyama, IEEE Trans. Radiat. Plasma Med. Sci. **6**, 592 (2022).

[9] H. Yoneda, H. Odaka, Y. Ichinohe, S. Takashima, T. Aramaki, K. Aoyama, J. Asaadi, L. Fabris, Y. Inoue, G. Karagiorgi, D. Khangulyan, M. Kimura, J. Leyva, R. Mukherjee, T. Nakasone, K. Perez, M. Sakurai, W. Seligman, M. Tanaka, N. Tsuji *et al.*, Astropart. Phys. **144**, 102765 (2023).

[10] M. H. L. Pryce and J. C. Ward, Nature (London) **160**, 435 (1947).

[11] H. S. Snyder, S. Pasternack, and J. Hornbostel, Am. Phys. Soc. **73**, 440 (1948).

[12] A. Strizhak, D. Abdurashitov, A. Baranov, A. Ivashkin, and S. Musin, Phys. Part. Nucl. Lett. **19**, 509 (2022).

[13] A. Selyem, C. Rosales-Guzmán, S. Croke, A. Forbes, and S. Franke-Arnold, Phys. Rev. A **100**, 063842 (2019).

[14] G. Jaeger, M. Teodorescu-Frumosu, A. Sergienko, B. E. A. Saleh, and M. C. Teich, Phys. Rev. A **67**, 032307 (2003).

[15] M. Żukowski, W. Laskowski, and M. Wieśniak, Phys. Rev. A **95**, 042113 (2017).

[16] M. T. L. Hsu, W. P. Bowen, and P. K. Lam, Phys. Rev. A **79**, 043825 (2009).

[17] K. Nogueira, J. B. R. Silva, J. R. Gonçalves, and H. M. Vasconcelos, Phys. Rev. A **87**, 043821 (2013).

[18] W. P. Bowen, N. Treps, R. Schnabel, and P. K. Lam, Phys. Rev. Lett. **89**, 253601 (2002).

[19] A. Wightman, Phys. Rev. **74**, 1813 (1948).

[20] U. Fano, J. Opt. Soc. Am. **39**, 859 (1949).

[21] W. H. McMaster, Rev. Mod. Phys. **33**, 8 (1961).

[22] G. Schmidt and L. M. Simons, Z. Phys. **263**, 387 (1973).

[23] H. Langhoff, Z. Phys. **160**, 186 (1960).

[24] L. R. Kasday, J. Ullman, and C. S. Wu, Nuovo Cim. B **25**, 633 (1975).

[25] A. R. Wilson, J. Lowe, and D. K. Butt, J. Phys. G **2**, 613 (1976).

[26] M. Bruno, M. D'Agostino, and C. Maroni, Nuov Cim. B **40**, 143 (1977).

[27] G. Bertolini, E. Diana, and A. Scotti, Nuov Cim. B **63**, 651 (1981).

[28] P. Caradonna, D. Reutens, T. Takahashi, S. Takeda, and V. Vegh, J. Phys. Commun. **3**, 105005 (2019).

[29] D. Abdurashitov, A. Baranov, D. Borisenko, F. Guber, A. Ivashkin, S. Morozov, S. Musin, A. Strizhak, I. Tkachev, V. Volkov, and B. Zhuikov, J. Instrum. **17**, P03010 (2022).

[30] S. Musin, A. Ivashkin, and A. Strizhak, Phys. Part. Nucl. Lett. **19**, 681 (2022).

[31] S. K. Sharma, D. Kumar, and P. Moskal, Acta Phys. Pol. A **142**, 428 (2022).

[32] P. Moskal, *2021 IEEE Nuclear Science Symposium and Medical Imaging Conference (NSS/MIC)* (2021), pp. 1–3.

[33] D. J. Bohm and B. J. Hiley, Nuovo Cim. B **35**, 137 (1976).

[34] D. Bohm and Y. Aharonov, Phys. Rev. **108**, 1070 (1957).

[35] S. Sofer, E. Strizhevsky, A. Schori, K. Tamasaku, and S. Shwartz, Phys. Rev. X **9**, 031033 (2019).

[36] E. Kuznetsova and O. Kocharovskaya, Nat. Photon. **11**, 685 (2017).

[37] A. Schori, D. Borodin, K. Tamasaku, and S. Shwartz, Phys. Rev. A **97**, 063804 (2018).

[38] A. Berera, Phys. Rev. D **102**, 063005 (2020).

[39] A. Berera and J. Calderón-Figueroa, Phys. Rev. D **105**, 123033 (2022).

[40] G. Torres del Castillo and I. Rubalcava-Garcia, Revista Mexicana de Fisica **57**, 406 (2011).

Correction: Equation (E1) contained a minor error and has been fixed.

Second Correction: A minor error in Eq. (38) has been fixed.